IEEE Access
Multidisciplinary | Rapid Review | Open Access Journal

SPECIAL SECTION ON NEW WAVEFORM DESIGN AND AIR-INTERFACE FOR FUTURE HETEROGENEOUS NETWORK TOWARDS 5G

Received September 18, 2019, accepted October 9, 2019, date of publication October 17, 2019, date of current version October 30, 2019.

Digital Object Identifier 10.1109/ACCESS.2019.2947992

On the Feasibility of 5G Slice Resource Allocation With Spectral Efficiency: A Probabilistic Characterization

J. J. ESCUDERO-GARZÁS[1], CARLOS BOUSOÑO-CALZÓN[2], AND ALFREDO GARCÍA[1]

[1]Department of Industrial and Systems Engineering, Texas A&M University, College Station, TX 77843, USA
[2]Department of Signal Theory and Communications, Universidad Carlos III de Madrid, 28911 Leganés, Spain

Corresponding author: J. J. Escudero-Garzás (jescugar@tamu.edu)

The work of J. J. Escudero-Garzás was supported in part by the Spanish National Project TERESA-ADA (MINECO/AEI/FEDER, UE) under Grant TEC2017-90093-C3-2-R, and in part by the National Spectrum Consortium, USA, under Project NSC-16-0140.

ABSTRACT An important concern that 5G networks face is supporting a wide range of services and use cases with heterogeneous requirements. Radio access network (RAN) *slices*, understood as isolated virtual networks that share a common infrastructure, are a possible answer to this very demanding scenario and enable virtual operators to provide differentiated services over independent logical entities. This article addresses the *feasibility* of forming 5G slices, answering the question of whether the available capacity (resources) is sufficient to satisfy slice requirements. As spectral efficiency is one of the key metrics in 5G networks, we introduce the *minislot-based slicing allocation* (MISA) model, a novel 5G slice resource allocation approach that combines the utilization of both complete slots (or physical resource blocks) and mini-slots with the adequate physical layer design and service requirement constraints. We advocate for a *probabilistic characterization* that allows to estimate feasibility and characterize the behavior of the constraints, while an exhaustive search is very computationally demanding and the methods to check feasibility provide no information on the constraints. In such a characterization, the concept of *phase transition* allows for the identification of a clear frontier between the feasible and infeasible regions. Our method relies on an adaptation of the Wang-Landau algorithm to determine the existence of, at least, one solution to the problem. The conducted simulations show a significant improvement in spectral efficiency and feasibility of the MISA approach compared to the slot-based formulation, the identification of the phase transition, and valuable results to characterize the satisfiability of the constraints.

INDEX TERMS 5G slice, resource allocation, feasibility, phase transition, Wang-Landau algorithm.

I. INTRODUCTION

In 5G networks, mobile operators face a challenging environment with the appearance of three new usage scenarios [1]. While enhanced Mobile Broadband (eMBB) services will provide very-high data-rate communications, some applications such as e-health or vehicular communications will demand Ultra Reliable Low Latency Communications (URLLC), which require very high reliability, very high security requirements, or both. In addition, a large number of objects (vehicles, appliances and many others) will be able to collect and transmit low-rate data through Massive Machine Type Communications (mMTC).

Mobile virtual network operators (MVO) or *tenants* are envisioned to provide these new services and will require new economically viable business models, as they find the cost of deploying 5G-compliant networks prohibitive. With the advent of 5G *multi-tenant* systems, MVOs can guarantee sufficient communication resources for 5G services at affordable cost. In the multi-tenant paradigm, the fundamental concept is the *network slice*, defined as a ''virtual network that is implemented on top of a physical network in a way that creates the illusion to the slice tenant of operating its own dedicated physical network.'' Reference [2] In other words, the resources corresponding to a common physical network are grouped and managed to form multiple logical, isolated networks that can be independently operated by different tenants [3], [4], so transforming the physical network into a set of heterogeneous virtual networks.

The associate editor coordinating the review of this manuscript and approving it for publication was Jinhwan Koh.

In forming *slices*, the infrastructure provider (InP) partitions the network such that each MVO's slice consists of a set of resources (e.g., spectrum, physical resource blocks, computation nodes) to meet the MVO's service requirements, so conferring a high level of flexibility upon 5G networks to deal with a large number of heterogeneous services and requirements [5]. However, slice resource allocation may lead to infeasible mathematical problems, causing opportunity costs for the MVOs and misuse of time and resources when they fail to form the slices. To avoid this undesirable situation, we propose a *probabilistic characterization of feasibility* that is particularly relevant to InPs and MVOs so that they can estimate the value of resources in advance and adjust payments and prices accordingly, as an alternative to dynamic pricing mechanisms [6].

On the other hand, 5G networks must provide high spectral efficiency [7]. To address efficiency, we propose the *minislot-based slicing allocation* (MISA) model to assign resources (physical resource blocks, PRBs) to eMBB and URLLC slices. The model combines physical (PHY) layer design with the use of minislots [8] and is formulated as an allocation problem where the constraints implement the system demands. The formulation includes service guarantee of bit error rate and data rate, and multiple-input multiple-output (MIMO) transmission, among other PHY layer characteristics. The resulting allocation problem (MISA-P) is a 0-1 nonlinear polynomial one where both the objective function and some constraints are polynomial,[1] which might be discussed in the context of linearization [9] or quadratization [10], [11]. However, there is no need to solve such a problem, as feasibility has all to do with the constraints, regardless of the objective function. Moreover, our study also contemplates characterizing the behavior of the unsatisfied constraints of MISA-P and the effect it may have on InPs and MVOs, and no optimization method would be able to perform such joint characterization. Hence, a resolution method to solve MISA-P is out of the scope of this work.

In this paper, we propose a *sampling-based approach* to estimate the feasibility of MISA-P and provide information about the unsatisfied constraints so that the results can be used by MVOs to make adjustments in case of infeasibility. In particular, we adapt the Wang-Landau algorithm, which has been broadly employed in Statistical Physics [12] and for constrained optimization problems [13]. In this way, we can predict the feasibility of the problem and the behavior of the constraints with negligible error, as our results show, see VI-C.

Regarding feasibility, the allocation of resources for network slices may exhibit a *phase transition*. A phase transition refers to an abrupt change in feasibility corresponding to a small change in one of the parameters, with a frontier delimiting the feasible and infeasible regions [14], [15]. The appearance of phase transitions has implications for efficient resource allocation as the search for optimal solutions becomes easier (respectively, harder) with sharp (respectively, smooth) phase transitions. Moreover, learning phase transitions in advance offers MVOs the possibility of rationalizing their resources, as a small number of additional resources may signify a much higher income for those points close to the frontier where a small change may revert a feasible problem to infeasible or vice versa.

In summary, the contribution of this work is twofold. On one hand, we propose a sampling method for systems with constraints that probabilistically characterize both feasibility and the satisfiability of the constraints. Second, we propose a new spectral-efficient approach to allocate PRBs for 5G slices to which the sampling method is applied.

The paper is organized as follows. Section II presents the related work and contributions. Section III introduces the system model and details slice specifications, the definition of the resources and the physical layer configuration. Section IV presents the formulation of the slice resource allocation. In Section V, we discuss the suitability of the sampling based approach. Section VI describes the adaptation of the Wang-Landau algorithm and its implementation. Section VII shows the simulation results the complexity analysis. Section VIII summarizes our conclusions.

II. RELATED WORK AND CONTRIBUTIONS–NEW

The interest in the study of 5G slicing has gathered momentum because of its prominent role to enable network sharing among InP and tenants [16]. In particular, the problem of how to efficiently allocate the available radio resources to slices has attracted significant attention and can be studied at different layer levels, as pointed out by Sallent *et al.* [17], [18] and in [19]. Strictly speaking, network slicing implies grouping network resources into different sets or *slices* with the objective of determining the number of resources that the slices require to meet service specifications, with allocated resources ranging from bandwidth to computing and storage [20]–[28] Nevertheless, a more global approach considers also the allocation of resources to users, i.e., the resources allocated to each slice are internally managed by its owner and assigned to final users. This allocation is known as *intra-slice allocation*, while the previous allocation of resources to slices is denoted as *inter-slice allocation*.

A. RADIO RESOURCE SLICING

Since slicing and network virtualization have been investigated, there has existed a generalized concern on how to share the available spectrum to form slices. The work of [29] performs channel allocation to maximize the sum-rate based on intra- and inter-slice priorities, while in [30], the authors adopt a market equilibrium perspective to virtualize the spectrum of a single BS. For a multiple cell setting, Parsaeefard *et al.* propose the joint user-BS association and user-channel allocation and incorporate power control to reduce inter-cell interference [31], where the non-convex mixed integer problem that guarantees the slice data rate is solved via a combination of complementary geometric

[1] We refer here to polynomials as terms of the form $\Pi_k x_k = x_1\, x_2 \ldots x_K$

programming and successive convex approximation. Other works contemplate cloud radio access network (C-RAN) scenarios [32], [33], sharing both licensed and unlicensed spectrum [34], or the coexistence of machine-type and classic cellular communications [35], [36]. To reflect an even more competitive market, the existence of multiple InPs is modelled in [37] to maximize the net revenue and in [38], where the BSs form coalitions to achieve a stable topology. Learning methods based on deep learning and reinforcement learning are designed for the periodic traffic prediction and spectrum allocation of the long-scale allocation and for the short-scale scheduling in [39], in the context of a two-time-scale slice dimensioning framework.

Besides spectrum slicing, other approaches appeared in the literature share the physical infrastructure. In [40], [41], a two-level hierarchical auction allocates the excess resources (subchannels, antennas and power) to tenants and users according to their bids. In [42], the authors study the partition of the antenna array of massive MIMO C-RAN radio remote heads (RRH), comprising also the association of users with baseband units (BBU). The RF infrastructure is sliced in [43], in which each MVO manages a set of RF chains through the different BSs. The work of [44] proposes a virtualization model based on allocating fractions of spectrum, caching storage and computing capacity to MVOs from multiple InPs.

However, the adoption of OFDM as the signal format for 5G has boosted the study of RAN slicing based on the allocation of PRBs (or RB), as defined in the OFDM frequency-time grid (see Fig.1). While a few studies differentiate intra- and iter-slice allocation [45], [46], the common approach for PRB-based slicing is the individual allocation of PRBs to users that belong to a slice/tenant/SP/MVO so as to simultaneously perform both allocations [47]–[53]. The model of [47] is based on service level agreements (SLA) and includes the allocation of power per PRB. A two-step approach is developed to solve the slicing problem in a tractable manner, allocating first PRBs to users under even power distribution over the PRBs and calculating the optimal power distribution for the resulting PRB allocation. The authors of [48] combine user scheduling, subcarrier power allocation, RB allocation, and non-orthogonal multiple access (NOMA) to maximize user's rate, while the stochastic framework proposed in [49] aims at minimizing the network power consumption with slice delay constraints. For a C-RAN in which the tenants have different priorities [50], the authors propose to resolve the association of users with RRHs and the allocation of processing capacity of BBUs, combined with the allocation of power to PRBs. Also for C-RAN, the scheme of [51] allocates PRBs to users at each time slot according to a bidding algorithm to minimize the usage of PRBs in the long term, subject to the constraints of capacity-critical and delay-critical slices. An interesting approach is presented in [52] to avoid the underutilization of resources due to strict isolation among slices, allowing that different tenants share the same PRB with a maximum intra-slice interference, with power allocation to control interference. For IoT communications, the work of [53] presents a nature-inspired resource allocation scheme that takes into account social characteristics.

Our paper intends to contribute with a new system model to perform intra- and inter-slice allocation of PRBs while gathering the constraints of URLLC and eMBB users. We observe that, though Quality of Service (QoS) requirements are in the essence of slicing, the design of transmission schemes or allocation algorithms to accommodate both eMBB and URLLC users is still little investigated. The works in [49], [51] adopt a stochastic approach to meet the QoS constraints in the long term and [54] propose an admission control perspective for the uplink. The work of [55] presents an optimization framework to associate eMBB and URLLC users with fog RAN (F-RAN) RRHs and to allocate subchannels to users to minimize the average delay of the URLLC users while guaranteeing a minimum data rate for the eMBB users, while [56], [57] introduce different service-oriented autonomous allocation algorithms based on deep reinforcement learning. However, none of these works formulates the allocation of different types of resources to users of different slices, i.e., mini-slots to URLLC users and PRBs to eMBB users, which leads to a significant improvement of the spectral efficiency.

B. FEASIBILITY OF RAN SLICING

In wireless networks in general, and for network slicing in particular, there are a number of random exogenous factors from the environment such as the number of users, rate demand, number of available channels, or signal-to-noise ratio, that complicate the task of determining feasibility in resource allocation problems. Note that the feasibility issue would be present (and not addressed) in most of the above mentioned works, as they solve constrained optimization problems where the uncertainty of the channel gain or the insufficient number of resources may render the problem infeasible.

Feasibility can be studied to provide evidence on the probability of solving the problem ex ante. For the 5G slicing context, this is somehow considered only by [58]–[61]. In [58], the authors establish the existence of a resource feasibility space as a previous condition to perform inter-slice allocation by means of a genetic algorithm. However, the determination of such a set is unspecified. In [59], two algorithms for slice admission that rely on space states given by the *admisibility region* are proposed. This region defines the number of elastic and inelastic users for which the slice is admitted according to several parameters such as traffic elasticity and price of the resources. The feasibility of the contracts between a MVO and InPs is analyzed in [60] with a single MVO that dominates the allocation, so defining a monopoly market, where the network is virtualized by associating users with the BSs of the different InPs. Our work is in some way aligned with the anticipatory resource scheduling proposed in [61], though the

model is different as they consider continuous time-sharing slicing.

In this regard, our contribution is a systematic study of feasibility of the slicing allocation problem according to the proposed MISA model. At first glance, our work is related to the K-SAT problem, in which there are M binary variables and each constraint is a polynomial of the form $x_1 x_2 \cdots x_K$, $K \leq M$ [62]. However, being the case that our constraints include also non-polynomial terms, the application of K-SAT-based methods is not possible. Other papers search for feasibility in the context of specific integer and mixed-integer problems, see for instance [63]–[65], but none of these two approaches provides a characterization of the constraints themselves. On the contrary, our probabilistic approach based on sampling methods provides both feasibility and constraints behavior. In particular, we adapt the Wang-Landau (WL) algorithm [12], an importance sampling method that compared with Monte Carlo methods makes it possible to detect rare events. The phase transition of the problem, which identifies the feasibility region, is obtained via the adapted WL algorithm.

The analysis of feasibility is based on random instances of the problem to include meaningful features of the communication environment, namely user position, signal-to-noise ratio, number of users per slice, and user's required data-rate.

TABLE 1. List of notations.

Symbol	Description
Δf	Sub-carrier bandwidth
N_{symbol}	OFDM symbols per resource block
N_{sub}	Sub-carriers per resource block
L	Mini-slots per slot
μ	Numerology
T_{slot}	Time-slot interval
$E(\sigma)$	Energy of configuration σ
f_o	Objective function
f	Wang-Landau multiplicative factor
G_m	Multiplicative factor of energy region $R(m)$
$g(E)$	Density of states with energy E
γ	Signal-to-noise ratio
γ_M	Signal-to-noise ratio threshold, modulation level M
BER	Bit error rate
k	User index
$\mathcal{K}, \mathcal{K}_1, \mathcal{K}_2$	Sets of total users, eMBB users and URLLC users
j	PRB index
m	Energy region index
η	Transmission efficiency of the OFDM symbol
Ω	$\{\mathbf{X}, \mathbf{y}, \mathbf{Z}\}$
$R(m)$	mth energy region
R_{eMBB}, R_{URLLC}	eMBB and URLLC slice rates
$r_k, \hat{r}_k$	Rate achieved and demanded by user k
σ	Configuration
t	Mini-slot index
$x_{k,j}, \mathbf{X}; \tilde{x}_{k,j}, \tilde{\mathbf{X}}$	Allocation of PRB j to user k, for MISA and SOSO
$y_j, \mathbf{y}$	Allocation of PRB j to URLLC users
$z^t_{k,j}, \mathbf{Z}$	Allocation of mini-slot t of PRB j to user k

III. SYSTEM MODEL

This section presents the service types addressed in this work and the PHY layer model that underlies the allocation problem formulated in Section IV. The notation used throughout this paper is shown in Table 1.

A. DESCRIPTION OF SERVICE TYPES

In 5G, three generic types of services will be supported [1], namely enhanced Mobile Broadband (eMBB), Ultra-Reliable and Low-Latency Communications (URLLC) for critical data, and massive Machine-Type Communications (mMTC). While eMBB services will support connections with very high data rates for applications such as multimedia content delivery, some critical applications such as e-health or vehicular communications will demand URLLC, implying very high reliability and/or very high security requirements. It is also expected that a large number of objects (smart grid meters, sensors, appliances and many others) will integrate communication capabilities to collect and exchange data making use of the Internet of Things (IoT) with mMTC.

It is evident that the three generic services aim at significantly differentiated scenarios and performance metrics, which translates into very different requirements. The goal of eMBB services is to maximize the data rate with moderate reliability, with connections that may be active for long periods of time. In the case of URLLC, there are strict requirements for metrics such as throughput, latency and availability, for a limited number of users that request connectivity with very diverse patterns. Finally, mMTC services are characterized by a massive number of intermittently connected devices typically transmitting low-rate, non-delay sensitive data.

This work discusses the case of eMBB and URLLC slices, not considering mMTC slices. There exists a consensus on reserving a low, fixed number of channels for the mMTC slice that the MTC devices share using a random access protocol [54]. As PRBs are allocated here on an orthogonal basis, there is no impact in the allocation of PRBs to eMBB and URLLC slices once the mMTC channels have been chosen.

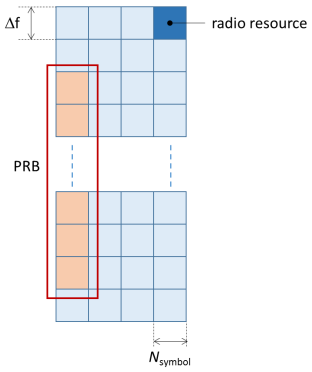

FIGURE 1. OFDM frequency-time grid.

B. NR FRAME STRUCTURE AND NUMEROLOGY

The radio resources in 5G NR are available in an OFDM-like manner (see Fig.1), where a frequency-time resource grid represents the system bandwidth (vertical axis) and the OFDM symbols (horizontal axis). Each radio resource corresponds to one sub-carrier of bandwidth Δf and one time-slot of N_{symbol} OFDM symbols. Additionally, slots can be divided

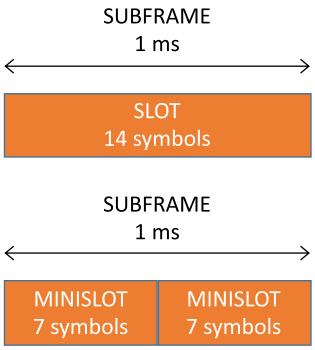

FIGURE 2. Minislot- and slot-based frames ($N_{symbol} = 14$).

into L mini-slots to accommodate traffic for URLLC services and facilitate very low latency and minimize interference to other RF bands [66]. Note that, to the best of our knowledge, previous works have considered the allocation of full PRBs to URLLC transmissions (e.g., [67]), leading to a loss of bandwidth efficiency, as the numerical results show in Section VII. Fig.2 illustrates the difference between the two frame structures for $\Delta f = 15$kHz.

TABLE 2. 5G NR numerology.

μ	Δf	Time-slot length
0	15 kHz	1 ms
1	30 kHz	0.5 ms
2	60 kHz	0.25 ms
3	120 kHz	0.125 ms
4	240 kHz	62.5 μs
5	480 kHz	31.25 μs

5G NR supports scalable numerology to address different requirements in terms of spectrum, bandwidth, deployment and services [68]. The choice of the numerology parameter μ implies a subcarrier space given by $\Delta f = \Delta f_0 \cdot 2^{\mu}$, being $\Delta f_0 = 15$ kHz (see Table 2), and a time-slot interval given by $T_{slot} = \frac{T_0}{2^{\mu}}$, where $T_0 = 1$ ms is the time-slot interval corresponding to $\mu = 0$. The number of OFDM symbols per time-slot is always 14, irrespective of the value of μ. The minimum resource allocation unit is however the physical resource block (PRB), which consists of 12 sub-carriers and one slot. Depending on μ, the bandwidth of one PRB ranges then from 180 kHz ($\mu = 0$) to 5.76 MHz ($\mu = 5$).

C. PHYSICAL LAYER PARAMETERS

Let us consider a single cell system with an eNodeB (eNB) in the center of the cell and K users randomly deployed. Let us define $\gamma_{k,j}$ as the signal-to-noise ratio (SNR) between the eNB and k over PRB j.

To guarantee quality of service, we fix a target bit error rate BER_0 for users. An adaptive modulation scheme is used to meet BER_0: for a given SNR γ, we adaptively select a modulation level among the available QPSK/16/64/256-QAM that satisfies $\gamma \geq \gamma_M$, being γ_M the SNR threshold corresponding to BER_0 and modulation of level M, where the BER can be calculated as [69]

$$BER = \frac{2\sqrt{M} - 3}{\sqrt{M}\log_2\sqrt{M}} \text{efrc}\left(\sqrt{\frac{3\log_2 M}{2(M-1)}\gamma}\right). \quad (1)$$

Although theoretically each PRB can be configured with a different modulation level, this would imply the design of transport channels in higher layers with the capacity of combining different modulation and coding schemes, which is not contemplated in 5G NR [70]. We therefore assume that, for a user k experiencing $\gamma_{k,j}$ on PRB j, all PRBs implement the same modulation level M_k, which corresponds to the lowest SNR over all PRBs, and the selected level is

$$M_k = \arg\min_M \{\gamma_{k,j} \geq \gamma_M, M = 4, 16, 64, 256\}. \quad (2)$$

We assume the use of 4×4 MIMO communications, $m = \log_2 M$ bits per baseband symbol, and let η denote the transmission efficiency of the OFDM symbol. Given these parameters, the transmission rate associated with one PRB is calculated as:

$$R_{PRB} = \frac{N_{sub} \cdot N_{symb} \cdot m \cdot \eta \cdot N_{MIMO}}{T_{slot}}, \quad (3)$$

where $N_{sub} = 12$ is the number of subcarriers per PRB, $N_{MIMO} = 4$ is the number of antennas for MIMO communications, and T_{slot} is the time-slot period. Then, the received data rate of user k on PRB j for the modulation scheme selected can be calculated as

$$r_{k,j} = R_{k,j}(1 - BER_0), \quad (4)$$

with $R_{k,j}$ given by (3). Note that such a characterization of the bit rate implicitly guarantees a quality of service in terms of BER, as all PRBs will be able to deliver the m bits with the target BER_0.

IV. THE RESOURCE ALLOCATION PROBLEM FOR EMBB AND URLLC SLICES

A. SLICE DESCRIPTION

In our model, two slices provide eMBB and URLLC services with total slice rates R_{eMBB} and R_{URLLC} respectively and allocate PRBs to users to satisfy their rate requirements $\hat{r}_k$, where $k \in \mathcal{K} = \{1, \ldots, K\}$ is the user index, $j \in \{1, \ldots, N\}$ is the PRB index, $\mathcal{K}_1$ denotes the set of eMBB users, and $\mathcal{K}_2$ the set of URLLC users, with $\mathcal{K} = \mathcal{K}_1 \cup \mathcal{K}_2$.

As the traffic patterns of both types of users are different [54], eMBB and URLLC users are allocated as many PRBs and mini-slots, respectively, as necessary to meet $\hat{r}_k$ for all users. In this way, the achieved data rate of eMBB users is given by

$$r_{k\in\mathcal{K}_1} = \sum_{j=1}^{N} x_{k,j} r_{k,j}, \quad (5)$$

where $x_{k,j} = 1$ denotes allocation of PRB j to user $k \in \mathcal{K}_1$ and $x_{k,j} = 0$ otherwise, with a total slice rate $R_{eMBB} = \sum_{k\in\mathcal{K}_1} r_k$. For the URLLC slice, we must take into consideration the

use of mini-slots. Without loss of generality, we set two mini-slots per PRB and the achieved data rate of URLLC users is given by

$$r_{k\in\mathcal{K}_2} = \sum_{j=1}^{N} y_j(z^1_{k,j} + z^2_{k,j})\frac{r_{k,j}}{2}, \tag{6}$$

where $y_j = 1$ denotes the use of PRB j for URLLC users and $y_j = 0$ otherwise, and $z^t_{k,j}$ represents the allocation of mini-slot $t = \{1, 2\}$ of PRB j to user $k \in \mathcal{K}_2$.

B. PROBLEM FORMULATION

Let denote by $\mathbf{X}$ the $K \times N$ eMBB allocation matrix whose elements are $x_{k,j}$, denote by $\mathbf{y}$ the URLLC allocation vector whose elements are y_j, and denote by $\mathbf{Z}$ the URLLC allocation array whose elements are $z^t_{j,k}$, with Ω representing the tuple $\{\mathbf{X}, \mathbf{y}, \mathbf{Z}\}$. The optimization problem to allocate PRBs to slices for any generic objective function $f_o(\Omega)$ can therefore be formulated as the minislot-based slicing allocation problem MISA-P:

$$\begin{aligned}
&\mathsf{opt}_{\Omega}\ f_o(\Omega) && \text{(MISA-P)}\\
&\text{s.t.}\quad r_k \geq \hat{r}_k, \quad \forall k \in \mathcal{K} && \text{(7a)}\\
&\qquad y_j + \sum_{k\in\mathcal{K}_1} x_{k,j} \leq 1, \quad \forall j && \text{(7b)}\\
&\qquad \sum_{k\in\mathcal{K}_2} (z^1_{k,j} + z^2_{k,j}) \leq 2y_j, \quad \forall j && \text{(7c)}\\
&\qquad y_j \in \{0, 1\}, \quad x_{j,k} \in \{0, 1\},\ z^t_{j,k} \in \{0, 1\}, && \text{(7d)}
\end{aligned}$$

where the token opt_{Ω} identifies the maximization max or minimization min framework over Ω. In this setting, the rates $\hat{r}_k$ demanded by users are assured by (7a), the orthogonal allocation of PRBs of (7b) guarantees isolation between the two slices, and the orthogonal allocation of mini-slots is guaranteed by (7c), allowing the assignment of both mini-slots to the same user.

The MISA-P formulation opens new possibilities with the use of mini-slots in 5G and its advantages will be shown in VII-B via exhaustive search with respect to the benchmark approach of IV-C. We want to emphasize that our interest lies in feasibility rather than proposing a method to solve any particular form of MISA-P with a specific objective function. The use of a generic $\mathsf{opt}_{\Omega}\ f_o(\Omega)$ obeys to the fact that feasibility has all to do with satisfying the constraints and nothing with the objective function. Therefore, solving the problem would be computationally inefficient as we want to check feasibility and characterize the satisfiability of the constraints. Moreover, for each $\mathsf{opt}_{\Omega}\ f_o(\Omega)$, a different optimization method should be proposed in case one decides to solve the problem.

C. BENCHMARK PROBLEM

To illustrate the spectral efficiency gain and the increase of feasibility of using mini-slots, we introduce the slot-based allocation problem (SOSO-P) that reflects the approach of previous works (see for instance [67]) and allocates full slots (PRBs) to users irrespective of the user is either eMBB or URLLC:

$$\begin{aligned}
&\mathsf{opt}_{\tilde{\mathbf{X}}}\ f_o(\tilde{\mathbf{X}}) && \text{(SOSO-P)}\\
&\text{s.t.}\quad r_k \geq \hat{r}_k, \quad \forall k && \text{(8a)}\\
&\qquad \sum_{k\in\mathcal{K}} \tilde{x}_{k,j} \leq 1, \quad \forall j && \text{(8b)}\\
&\qquad \tilde{x}_{k,j} \in \{0, 1\}. && \text{(8c)}
\end{aligned}$$

In this formulation, $\tilde{x}_{k,j}$ are the elements of $\tilde{\mathbf{X}}$ denoting the allocation of PRB j to user k, $f_o(\tilde{\mathbf{X}})$ represents a generic optimization function, the token $\mathsf{opt}_{\tilde{\mathbf{X}}}$ identifies the maximization max or minimization min framework over $\tilde{\mathbf{X}}$, and the user and slice rates are now

$$\tilde{R}_s = \sum_{k\in\mathcal{K}_s} \tilde{r}_k \tag{9}$$

$$\tilde{r}_k = \sum_{j}^{N} \tilde{x}_{k,j} r_{k,j}, \quad k \in \mathcal{K}_s \tag{10}$$

$$s = \{1, 2\}. \tag{11}$$

V. FEASIBILITY OF MISA-P

As we mention in the introduction, we turn to the concept of phase transition for the characterization of the feasibility of MISA-P. This concept applies to a geometrical element (plane, curve, line) that allows us to experimentally differentiate the feasible and infeasible regions.

MISA-P is a 0-1 nonlinear, polynomial problem as the constraints (7a) are polynomial due to the terms $y_j(z^1_{k,j} + z^2_{k,j})$. Furthermore, for a wide range of usual network problems such as the maximization of the sum-rate where $\mathsf{opt}_{\Omega} f_o(\Omega) = \max \sum_{k=1}^{K} r_k$, the polynomial terms are also in the objective function, rendering the problem more difficult to solve (see [71], p.611). The resolution of MISA-P may be discussed in the context of linearization [9] or quadratization [10], [11]. However, as we mention in IV-B, proposing a method to solve MISA-P is out of our scope, being the ultimate objectives i) to show that there exists a phase transition that can be exploited by the MVOs to, for example, adjust the requirements to turn the resource allocation into feasible; and ii) to characterize the satisfiability of the constraints.

Among the approaches that can be used to check feasibility, the bisection method [72] may be adapted for pure 0-1 problems, but is does not provide any information about constraint satisfiability and the density of states (the number of solutions that do not satisfy a given number of constraints). The exact characterization of the phase transition for MISA-P comprises both feasibility and constraints and would imply an exhaustive search over all the possible solutions $\omega \in \Omega$ to determine which ω meet the constraints (7a)–(7c). Unfortunately, this strategy is computationally intractable in practice. Let us take for instance the case of $K_1 = 2$ eMBB users, $K_2 = 3$ URLLC users and $N = 10$, implying that the number of variables is $V = N(K_1 + 2K_2 + 1) = 90$ and being therefore the number of possible solutions to be tested

$2^{90} \approx 1.24 \times 10^{27}$. In our experiments, the computational time to check each potential solution is 0.5 ms on a PC, what leads to a total time of 7.164×10^{18} days. Moreover, the characterization must also account for the random nature of i) the users' position, which implies a random modulation scheme selection via SNR; ii) type and number of users; and iii) demanded data rate. This implies that a sufficient number of random realizations of the same instance $\{K_1, K_2, N\}$ of the problem must be evaluated to achieve credible results.

It is then clear that a method which does not require exhaustive search is imperative. Alternatively, the phase transition and constraints satisfiability can be characterized in a probabilistic fashion via a sampling method such as the Wang-Landau algorithm. In the next section, we describe this algorithm and the modifications required for our problem.

VI. THE DENSITY OF STATES FOR SLICES ALGORITHM

In this section, we develop the density of states for slices (DESS) algorithm, which is based on the Wang-Landau algorithm, to characterize the feasibility of (MISA-P). The Wang-Landau (WL) method is a non-Markovian Monte Carlo approach [12] to estimate the density of states of Physics systems. Compared with Metropolis-based methods [73], the WL algorithm allows to sample the search space in less time while preserving accuracy and efficiency and has been employed for many other applications, from the folding of proteins [74] to the estimation of interference in wireless networks [75]. As a specific jargon is used in the related literature, we provide the following definitions:

- *State*: represents a level of energy.
- *Configuration,* σ: each element of the solution space of the problem. In our case, it refers to any possible value of $\mathbf{X}$, $\mathbf{y}$ and $\mathbf{Z}$.
- *Energy of a configuration,* E: it represents how good the configuration is as a solution to the problem. In this paper, the energy of a configuration $E(\sigma)$ is the number of constraints of MISA-P not satisfied by σ.
- *Density of states,* $g(E)$: estimate of the number of configurations with a given energy E. In this paper, it corresponds to the number of solutions (configurations) that do not satisfy a certain number of constraints of the problem.

Therefore, a configuration with zero energy $E(\sigma) = 0$ satisfies all the constraints, and $g(0)$ is the number of solutions to the problem. As an example, for a 2-state system with possible energy levels $E = \{0, 1\}$, $g(1) = 10$ means that there are 10 configurations from the solution space that do not satisfy one of the constraints, while $g(0) = 2$ means that there exist 2 configurations that satisfy all the constraints, implying that there are two solutions to the problem.

Remark: According to the above definitions, we declare a given realization of our problem as **feasible** if $g(0) > 0$, and infeasible otherwise. This is the criteria that will be used to establish the phase transition, as it means that there exists, at least, one solution to the problem.

A. BASICS OF THE WANG-LANDAU ALGORITHM

For the sake of completeness, this subsection summarizes the principal steps of the WL algorithm [12].

The WL algorithm works performing a number of random walks in our configuration space $\{0, 1\}^V$. When a new configuration σ with energy E_i is proposed, the new state is accepted with a probability proportional to the reciprocal of the density of E_i. During the random walk, the histogram $H(E)$ keeps the number of visits at each energy level E_i and $H(E_i)$ is incremented by 1 each time E_i is visited. For each random walk, the estimate of the density of states is modified by a factor f, and the updated density of states is used to perform a new random walk. With this setting, each random walk generates a flat histogram for the energy distribution based on the observation that, if the configurations σ are sampled with probability proportional to $1/g(E)$, the resulting histogram is flat.

Let us denote by σ_1 and σ_2 the current and new configurations, and $E_1 = E(\sigma_1)$ and $E_2 = E(\sigma_2)$ the corresponding energies. The transition probability from σ_1 to σ_2 is

$$p(\sigma_1 \rightarrow \sigma_2) = \min\left(1, \frac{g(E_1)}{g(E_2)}\right), \tag{12}$$

which implies that the state with energy E_2 is accepted if $g(E_1) \geq g(E_2)$; otherwise, the state with energy E_2 is accepted with probability $g(E_1)/g(E_2)$. After this, the density of state of E_2 is adjusted by the multiplicative factor f such that $g(E_2) \rightarrow f \times g(E_2)$ and the energy histogram is accordingly updated, i.e. $H(E_2) \rightarrow H(E_2) + 1$ if E_2 is accepted and $H(E_1) \rightarrow H(E_1) + 1$ otherwise. In practice, logarithmic scale is used to compute $g(E)$ since these values may become extremely large; therefore, each update is implemented as $\log(g(E)) \rightarrow \log(f) + \log(g(E_2))$.

The value of f usually starts at $f = e$ and is updated by $f \rightarrow \sqrt{f}$ each time we get a flat histogram (i.e., the algorithm converges for that f) before generating a new random walk. Random walks are generated until $f = 1$ with an error of 10^{-8}, as at this point we would have the true density. With these values, 27 random walks are generated.

At the end of the simulation, the algorithm provides a density of states relative to the total number of visited states, which is much smaller than the total. To extract the correct density, we need to scale to the total number of states 2^V, where V represents the number of variables of the problem.

B. THE DESS ALGORITHM

Given that the WL algorithm is designed to evaluate continuous densities of states and our problem is eminently discrete, some modifications are required to adapt the WL method to MISA-P. We refer to the adapted algorithm as the modified WL algorithm for slices (MWLS) and its pseudocode is given in Algorithm 1, which integrates these modifications with the basics of VI-A and where $\mathbf{\Omega}_c$ represents a potential solution or configuration of MISA-P.

Determining the density of states for very-low energy regions poses two challenges. The first issue is the huge

Algorithm 1 Modified Wang-Landau for Slices (MWLS)

Data: initial state E_1, f_{limit}, SNR, K_1, K_2
Result: Density of states $\mathbf{g}$
1 Define energy regions $R(m)$
2 **for** *each* $R(m)$ **do**
3 **while** $f - 1 > f_{limit}$ **do**
4 **while** $\mathbf{h}_m$ *not flat* **do**
5 new configuration $\mathbf{\Omega}_c = \text{GEN}(K, N)$;
 calculate the energy $E_2(\mathbf{\Omega}_c)$ with (7a)–(7c)
6 calculate probability p from (12)
7 **if** $p = 1$ **then**
8 accept new state E_2
9 **else**
10 $E_2 \leftarrow E_1$
11 **end**
12 update density, histogram and E_1:
13 $\tilde{g}_m(E_2) + \log f \leftarrow \tilde{g}_m(E_2)$
14 $h_m(E_2) + 1 \leftarrow h_m(E_2)$
15 $E_1 \leftarrow E_2$
16 check if $\mathbf{h}_m$ is flat
17 **end**
18 $\sqrt{f} \leftarrow f$
19 check $f - 1 > f_{limit}$
20 **end**
21 calculate multiplicative factor G_m for $R(m)$
22 update $\tilde{\mathbf{g}}$ until $R(m)$
23 **end**
24 construct true estimate $\mathbf{g}$ from $\tilde{\mathbf{g}}$
25 scale $\mathbf{g}$

discrepancy between the density of the states corresponding to the energy bound regions (states with $E = \{E_{min}, E_{max}\}$ and close values) and the density of the central states, difference that can reach several orders of magnitude. As suggested in [76], we have implemented a per-region calculation, dividing the whole region $E = [E_{min}, E_{max}]$ into smaller regions $R(m) = [E^m_{min}, E^m_{max}]$ that partially overlap and calculating the density of states independently for each region. The true estimated density is obtained by matching the overlapping values, what provides a multiplicative factor that is applied to the subsequent densities of the upper region. For instance, let be a setting with two adjacent regions $R(1) = [E_0, \ldots, E']$, $R(2) = [E', \ldots, E_T]$ which overlap in E' and the corresponding densities $\tilde{\mathbf{g}}_1, \tilde{\mathbf{g}}_2$. Assuming that $\tilde{g}_1(E') = 1$, $\tilde{g}_2(E') = 2$, the multiplicative factor is $G_1 = \frac{\tilde{g}_1(E')}{\tilde{g}_2(E')} = 2$, and the true estimated density is

$$\mathbf{g}(E) = \begin{cases} G_1 \times \tilde{\mathbf{g}}_1(E) & \forall E \in R(1) \\ \tilde{\mathbf{g}}_2(E) & \forall E \in R(2), \quad E > E'. \end{cases}$$

We then define the multiplicative factor for region $R(m)$ as

$$G_m = \frac{\tilde{g}_{m-1}(E')}{\tilde{g}_m(E')}, \tag{13}$$

where the two consecutive regions overlap in E'. The corresponding update is found in lines 22–23 of Algorithm 1 for the energy regions loop (lines 2–24).

The second critical issue regarding the low energy regions is the determination of the energy levels for which no configuration exists, as such energy levels would never be visited and the algorithm would not converge. The self-adapting energy range from [77] avoids this problem by considering only certain energy levels to evaluate the flatness of $H(E)$. However, given that we have previously defined the fixed energy regions $R(m)$, we propose the GEN algorithm (see Algorithm 2) to randomly generate a candidate configuration $\mathbf{\Omega}_c$ with energy E_c for $R(m)$, and $\mathbf{\Omega}_c$ is accepted if it belongs to the region, i.e., $E_c \in R(m)$. Otherwise, we repeat the random generation until success or until a sufficient number of trials is reached.

Algorithm 2 Generation of Valid Configuration (GEN)

Data: Energy region $R(m)$, t_{max}
Result: Candidate configuration σ_c
while $\Omega_c \notin R(m)$ **do**
 Randomly generate new σ_c
 $t \leftarrow t + 1$
 if $t = t_{max}$ **then**
 exit
 end
end

We now face the criteria to evaluate flatness. In their original paper [12], Wang and Landau define ''flat histogram'' as a histogram $H(E)$ whose values are at least 80% of the average histogram. However, different authors have discussed other criteria for ''flatness'' to better capture the specific conditions of other models. In particular, some energy values may be visited very few times, leading to convergence uncertainty to achieve a flat H. We have implemented the criteria of [76], where each state is visited a minimum number of times unless it is declared a state with density 0 by the GEN algorithm or a maximum number of iterations is reached. In our case, we determined experimentally that the required number of visits is $3KN$ and the maximum number of iterations is $KN \times 10^3$. Other suitable flatness criterion [77], [78] were tested, with worse performance in terms of error when confronted with the exhaustive search results (true density).

The above procedures are integrated in the main algorithm DESS (see Algorithm 3), which is designed to capture the randomness of our problem. Indeed, a single run of the MWLS algorithm may not provide accurate results, given the random nature of the wireless medium, which encompasses pathloss, user mobility, user's required rate, and number of users per service type. To get reliable results, we have established the converge of the algorithm in the density of states as follows. Firs, we fix the required user rates and the number of users per service type K_1 and K_2. At each iteration of the *while* loop (line 1), the users are randomly positioned to obtain

Algorithm 3 Density of States for Slices (DESS)

Data: demand rates $\hat{\mathbf{r}}$, number of users per service type K_1, K_2
Result: Density of states $\mathbf{g}$

1 **while** $\epsilon > \epsilon_0$ **do**
2 calculate new SNR values: $\Gamma = \{\gamma_{k,j}\ \forall k, j\}$
3 calculate new $\mathbf{g}_t = \text{MWLS}(\Gamma, K_1, K_2)$
4 $t \leftarrow t + 1$
5 evaluate ϵ
6 **end**

a new set of SNR values Γ (line 2). A new density of states $\mathbf{g}_t(E)$ is calculated until the difference between the average of the sequence $\{\mathbf{g}_1, \ldots, \mathbf{g}_{t-1}\}$ and the average of the sequence $\{\mathbf{g}_1, \ldots, \mathbf{g}_t\}$ is less than ϵ, i.e., the algorithm converges.

C. ACCURACY OF THE DESS ALGORITHM

To assess the precision of the DESS algorithm, we have compared it with the exact solution obtained with exhaustive search. Fig.3 displays the density of states with both methods, where we observe that the curves overlap with the exception of a small discrepancy in the upper bound for the case $K = 3$, $N = 6$. The parameters used here are the same detailed in Table 3.

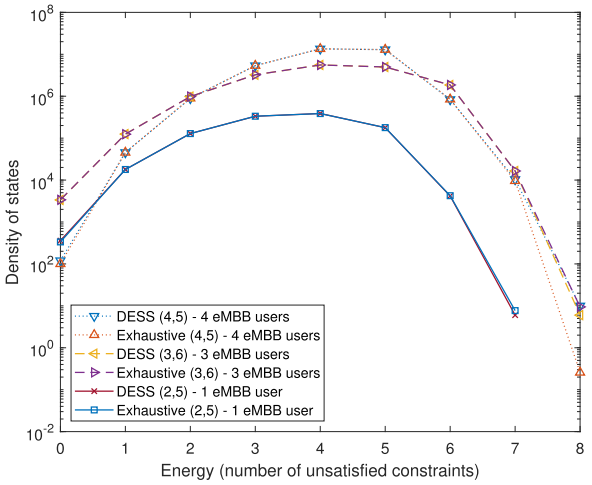

FIGURE 3. Wang-Landau versus exhaustive search.

Alternatively to the use of $f = \sqrt{f}$, two strategies represent the state of the art in the control of accuracy for Wang-Landau algorithms [79], the WL-$1/t$ algorithm and the stochastic approximation Monte Carlo (SAMC) algorithm. The WL-$1/t$ algorithm [80] defines the time when the 1/t regime starts as the time when all energy levels have been visited at least once. However, some instances of our problem are characterized by true energy levels that are never visited, making the application of this strategy impossible. The SAMC algorithm [81] specifies that, in practice, the time t_0 when the $1/t$ regime

TABLE 3. Parameter values for simulation.

Parameter	Value
Number of users K	2–5
Number of PRBs, N	2-6 (for $K = 2, N =$ 1–6)
Transmit power per PRB, P	0.2 W
Path loss, PL[dB]	$20\log(d) + 20\log(f) + 92.4 + \sigma$
Distance user-eNB, d[km]	$\sim \mathcal{U}[0.1, \sqrt{2}]$
Shadowing effect, σ [83]	$\sim \mathcal{N}(0, 6.7)$
PRB carrier frequency, f	$f_0 + nN_{sub}\Delta f,\ n = 1, \ldots, N$
f_0	3.5 GHz
BER	10^{-3} (eMBB), 10^{-8} (URLLC)
DESS convergence, ϵ	10^{-2} (1%)
Numerology, μ	4

starts is chosen according to the complexity of the problem, and the appropriateness of the choice of t_0 is determined by testing the convergence of multiple runs by examining the variation of the estimated density of states. For our problem, this approach would mean the design of t_0 for each instance of the random parameters involved (number of eMBB users, number of URLLC users, signal-to-noise ratio, number of PRBs), implying the determination of more than 250 values (50 iterations with at least 5 iterations for the DESS algorithm) of t_0 per (K, N) pair, which is very impractical and highly time consuming.

The error corresponding to Fig.3 is calculated as in [80] for $(K, N) = (2, 5), (3, 6), (4, 5)$, with values $1 \cdot 10^{-2}$, $4.5 \cdot 10^{-5}$, $6 \cdot 10^{-6}$, respectively, which are consistent with the values reported for $f = \sqrt{f}$ in other works (see for instance [80].) These results are a very good compromise between accuracy and the complexity exhibited by our DSSS algorithm, which is shown in VII-E to scale with $\mathcal{O}(V^{4.11})$ while the 2D Ising model of [82] scales with $\mathcal{O}(V^{4.743})$.

VII. EXPERIMENTS AND EMPIRICAL RESULTS

A. SIMULATION SETTING

The wireless configuration consists of an eNodeB that covers a square area of of 2×2 km^2 and users randomly positioned following a uniform distribution in a free space scenario with line of sight where the shadowing effect is given by the random variable σ. The remaining parameters are provided in Table 3 and in III-B.

The simulations conducted to provide the feasibility results have been obtained as follows. We have generated 50 independent instances for each pair (K, N), each instance corresponding to one execution of the DESS algorithm. For each instance, the parameters are:

- number of users per slice: $K_1 = K - \kappa$ and $K_2 = \kappa$, being κ a uniform integer random variable in $[0, K]$;
- path loss realizations are randomly generated (see Table 3) for each instance to obtain different sets of SNR until convergence of the density distribution in ϵ;
- user rate demands $\hat{\mathbf{r}}_k$ [Mbps] are chosen from a uniform distribution $\mathcal{U}[15, 30]$ for eMBB users and uniform distribution $\mathcal{U}$ for URLLC users.

B. COMPARISON BETWEEN THE MISA-P AND THE SOSO-P MODELS

This section shows the performance that the two models exhibit for two meaningful scenarios in which the number of available PRBs is i) equal to the number of users and ii) less than the number of users. These results have been obtained by exhaustive search.

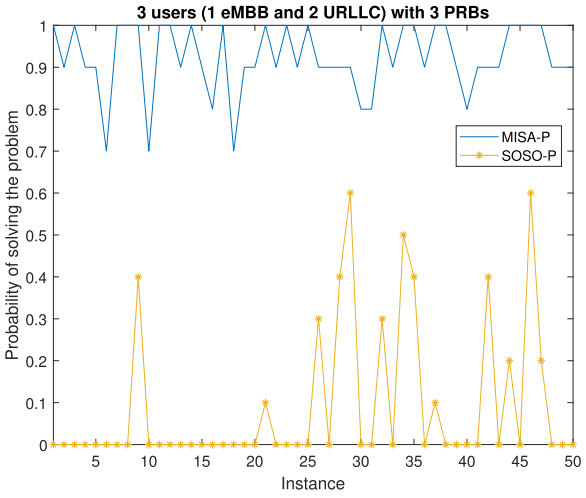

(a) K=3, N=3

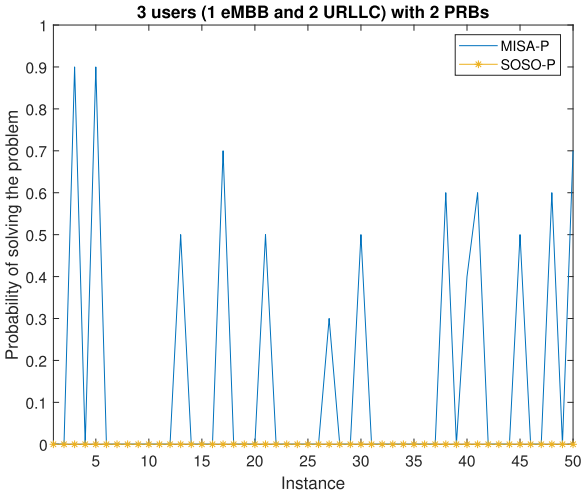

(b) K=3, N=2

FIGURE 4. Probability of existence of solution.

The fact that two URLLC users can be allocated different mini-slots implies a significant improvement in feasibility, as Fig.4 shows for the case of 3 users, of which one demands eMBB service and two demand URLLC service. If 3 PRBs are available (Fig.4a), it is clear that there is no guarantee that the problem is feasible, depending on the SNR of the PRBs and the rates demanded by the users. Indeed, we see that the MISA-P model provides a probability of feasibility between 70% and 100%, while the SOSO-P model is infeasible for many instances with a maximum probability of feasibility of 60%. If we stress the models further and reduce the number of PRBs to 2, the MISA-P model is still feasible in some cases while the SOSO-P model is always infeasible as the number of users exceeds the number of PRBs (Fig.4b).

Regarding the performance in terms of bandwidth efficiency, we have studied the maximization of the achieved sum-rate as a meaningful example that contains all the variables of the MISA approach, i.e. $x_{k,j}$, y_j, and $z^t_{k,j}$, yielding the two following objective functions:

$$\begin{aligned}\mathsf{opt}_{\Omega}\, f_o(\Omega) &= \max \sum_{k=1}^{K} r_k \\ &= \max \sum_{k=1}^{K_1}\sum_{j=1}^{N} x_{k,j} r_{k,j} \\ &\quad + \sum_{k=1}^{K_2}\sum_{j=1}^{N} y_j (z^1_{k,j} + z^2_{k,j}) \frac{r_{k,j}}{2} \qquad \text{(MISA-P)}\end{aligned}$$

$$\mathsf{opt}_{\tilde{\mathbf{X}}}\, f_o(\tilde{\mathbf{X}}) = \max \sum_{k=1}^{K} \tilde{r}_k = \max \sum_{k=1}^{K}\sum_{j}^{N} \tilde{x}_{k,j} r_{k,j} \qquad \text{(SOSO-P)}$$

The results in Figs.(5a)-(5b), for the same two cases that for Fig.4, show the bandwidth efficiency for the two models. Note that there is a remarkable difference between the efficiency provided by MISA-P with respect to SOSO-P, being at least $2\times$ for $K = 3, N = 3$ and infinite for $K = 3, N = 2$, as SOSO-P is always infeasible in this case.

C. CHARACTERIZATION OF FEASIBILITY

The probabilistic characterization of feasibility for the slice problem is now shown. We recall that feasibility means that the number of solutions to the problem is larger than 0, i.e., $g(0) > 0$. Fig.6 displays the probability that the problem is feasible as a function of slice rates per available PRB $\frac{R_s}{N}$, where each point corresponds to one of the 50 instances for each (K, N) with the DESS algorithm. We observe that there is a trade-off between R_{eMBB} and R_{URLLC} that delimits the feasible and infeasible regions, which are defined by the orange curve. This graphic may then be used to know how feasible will be the slicing problem in advance. Feasibility can be characterized in more detail via the cumulative density function (CDF) of Fig.7, for different number of users. This figure makes it explicit the effect of an insufficient number of resources: while for 2 users feasibility is very high, feasibility for 5 users is much lower, given that the maximum number of available PRBs is 6.

Fig.8 shows the CDF for the average of satisfied demanded rate $\hat{r}$, for which the probability of feasibility has been taken into consideration. Note that, for each type of service, the curves are very close, meaning that, in average, users get the same rate irrespective of the number of users present in the system. As similar curves were obtained for all values of K, we choose to reproduce $K = 2$ and $K = 4$ for a better visualization of the curves.

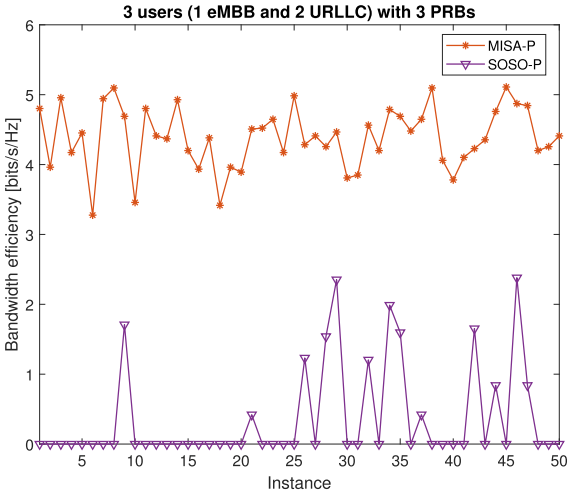

(a) K=3, N=3

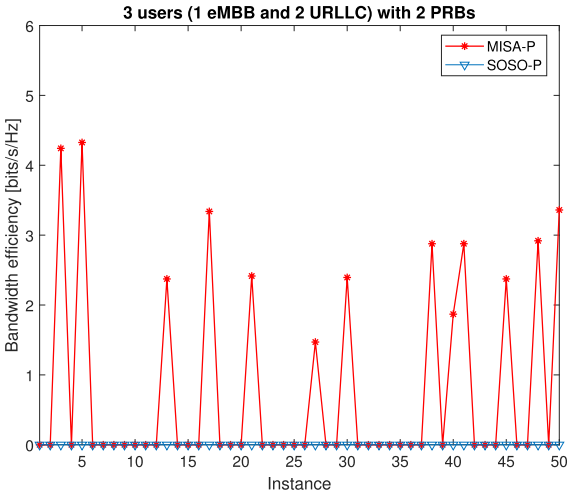

(b) K=3, N=2

FIGURE 5. BW efficiency: Comparison between MISA-P and SOSO-P to maximize the sum-rate.

TABLE 4. Average number of constraints that are unsatisfied, for $N = 4$. The figures correspond to non-scaled values.

Constraint-PRB	$K = 3$	$K = 4$
(7b)-1	0.7733×10^5	1.3296×10^5
(7b)-2	0.7732×10^5	1.3295×10^5
(7b)-3	0.7733×10^5	1.3294×10^5
(7b)-4	0.7733×10^5	1.3295×10^5
(7c)-1	1.0921×10^5	1.8153×10^5
(7c)-2	1.0922×10^5	1.8153×10^5
(7c)-3	1.0921×10^5	1.8152×10^5
(7c)-4	1.0921×10^5	1.8152×10^5

D. CONSTRAINTS ANALYSIS

The density of states is also used to evaluate the behaviour of the constraints, by registering which constraints are unsatisfied. Our first observation is that all constraints of the same type have very similar values for each (K, N), as Table 4 shows. Moreover, we see that the constraints regarding the use of mini-slots (7c) are more restrictive than the constraints on slice isolation (7b), showing that orthogonality between URLLC users using the same PRB is more stringent that orthogonality between the eMBB and URLLC slices.

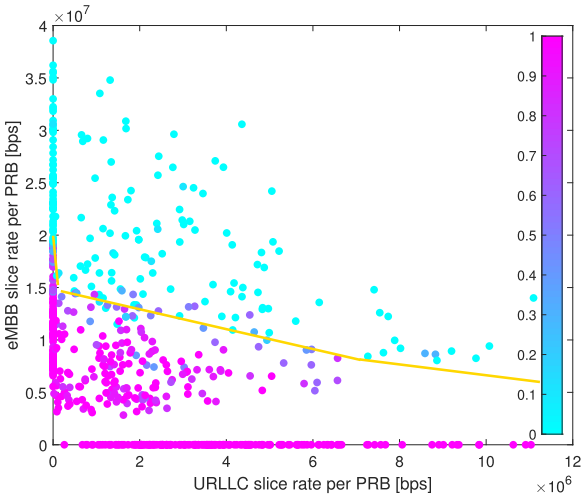

FIGURE 6. Phase transition as a function of $\frac{R_{eMBB}}{N}$ and $\frac{R_{URLLC}}{N}$.

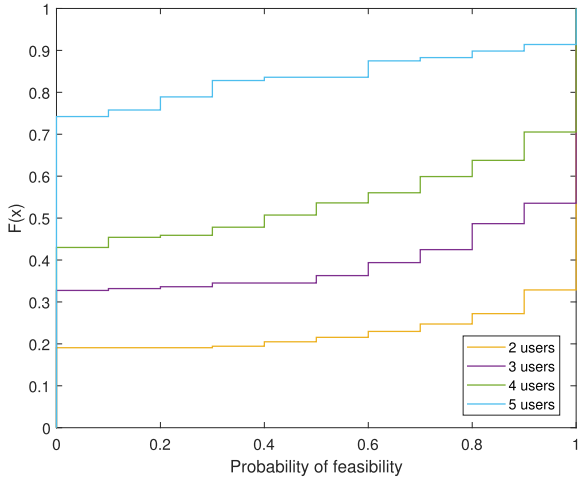

FIGURE 7. Feasibility (CDF).

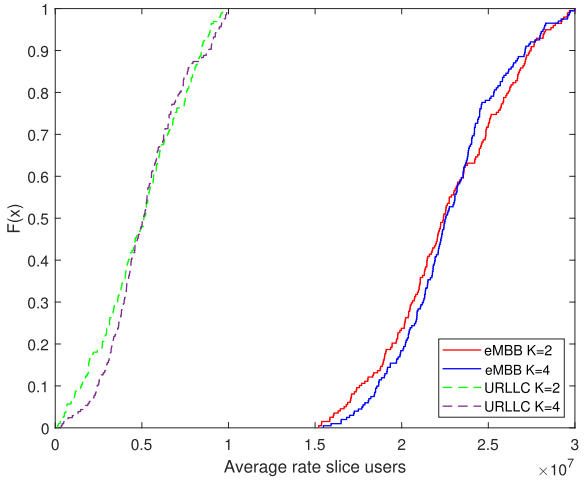

FIGURE 8. Average users rate per slice (CDF).

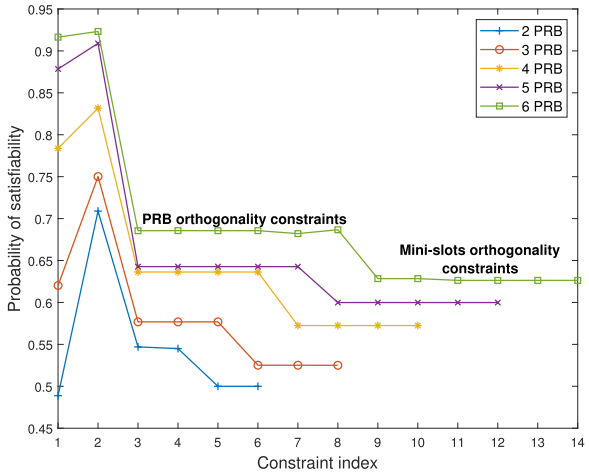

FIGURE 9. Probability of satisfiability of the constraints, for $K = 3$. The curves are limited in the x-axis to the number of constraints $2N + 2$.

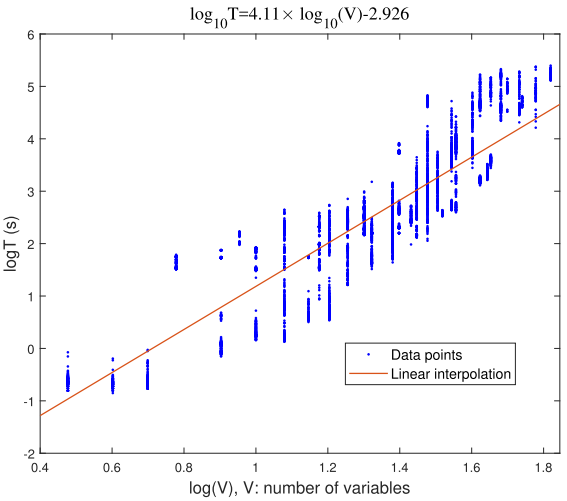

FIGURE 10. Complexity of the modified MWLS algorithm: logarithm of the computational time T as a function of the number of variables $V = N(K_1 + 2K_2 + 1)$, K_1 is the number of eMBB users, K_2 is the number of URLLC users.

We can also estimate the probability of satisfiability of each constraint, where the x-axis represents the constraint index such that $x = 1$ stands for constraint#1 and so on, for the case of $N = 3$, see Fig.9. Regarding the fulfillment of slice data rates, constraints 1 and 2 ($x = 1$ and $x = 2$) map the satisfaction of the requirements of the eMBB and URLLC slices, respectively, once it has been guaranteed that user requirements (7a) are satisfied. Put differently, $x = 1$ and $x = 2$ represents the probabilities $P\{r_k \geq \hat{r}_k,\ \forall k \in \mathcal{K}_1\}$ and $P\{r_k \geq \hat{r}_k,\ \forall k \in \mathcal{K}_2\}$ for all eMBB and URLLC users, respectively. We observe that the larger the number of PRBs, the higher the probability for both types of users, achieving values of around 90% for $N = 6$. Note that for 2 PRBs, which is less than the number of users, the probabilities for $x = \{1, 2\}$ are respectively $\{50\%, 70\%\}$ and therefore not null, as it would be the case with conventional approaches such as SISO-P. We also see the evolution of the orthogonality constraints (7b)–(7c), which correspond to the flat parts of the curves and labelled for the curve '6 PRB' in the figure, showing that increasing probabilities accompanies the increase in the number of PRBs.

E. COMPLEXITY ANALYSIS

We now analyze the computational complexity of the MWLS algorithm. The complexity is estimated taking into account the obtained simulation times and following recent advances in the estimation of how the computational time scales with the number of variables in Wang-Landau algorithms [79], [82]. In these works, Shchur *et al.* show that the simulation time scales with V^z, being V the number of total variables and z a problem-specific parameter which changes depending on the particular problem. Fig.10 shows, in logarithmic scale, the simulation time T versus the number of variables V. These data can be approximated by the line $\log_{10} T = 4.11 \times \log_{10}(V) - 2.926$, giving a value $z = 4.11$ that implies a complexity $\mathcal{O}(V^{4.11})$. We observe that in [82] values of z in the range $[4, 5.7]$ are reported for the tunneling time, which matches our convergence criteria, suggesting that our modified Wang-Landau algorithm scales better than the 2D Ising model with $z = 4.743$. Note that the total complexity of the DESS algorithm is simply $\alpha\mathcal{O}(V^{4.11})$, being α the number of times that the MWLS is executed (see Table 3, *while* loop); in our experiments, $\alpha = [5, 10]$.

VIII. CONCLUSION

This paper proposes the probabilistic characterization of feasibility of 5G slice resource allocation problems to a priori discern whether they can be solved or not. In particular, we present MISA-P, a novel spectral-efficient approach to the allocation of PRBs for eMBB and URLLC services based on the utilization of minislots. We have adapted the Wang-Landau algorithm to our scenario to characterize the satisfiability of the constraints and to obtain the phase transition that delimits the feasible and infeasible slice rate regions. This characterization makes it possible for slice owners to learn in advance whether the number of resources is adequate to provide the required data rates and to anticipate actions that avoid an unsuccessful allocation process. We also show that our approach significantly improves the spectral efficiency with respect to a single-slot based model.

REFERENCES

[1] *IMT Vision—Framework and Overall Objectives of the Future Development of IMT for 2020 and Beyond*, doucument Rec. ITU-R M.2083, 2015. Accessed: Sep. 13, 2018. [Online]. Available: https://www.itu.int/dms_pubrec/itu-r/rec/m/R-REC-M.2083-0-201509-I!!PDF-E.pdf

[2] S. Vassilaras, L. Gkatzikis, N. Liakopoulos, I. N. Stiakogiannakis, M. Qi, L. Shi, L. Liu, M. Debbah, and G. S. Paschos,"The algorithmic aspects of network slicing," *IEEE Commun. Mag.*, vol. 55, no. 8, pp. 112–119, Aug. 2017.

[3] *Feasibility Study on New Services and Markets Technology Enablers; Stage 1*, document 3GPP TR22.891 v2.0.0., 2016.

[4] P. Muñoz, O. Sallent, and J. Pérez-Romero, "Self-dimensioning and planning of small cell capacity in multitenant 5G networks," *IEEE Trans. Veh. Technol.*, vol. 67, no. 5, pp. 4552–4564, May 2018.

[5] P. Rost, C. Mannweiler, D. S. Michalopoulos, C. Sartori, V. Sciancalepore, N. Sastry, O. Holland, S. Tayade, B. Han, D. Bega, D. Aziz, and H. Bakker, "Network slicing to enable scalability and flexibility in 5G mobile networks," *IEEE Commun. Mag.*, vol. 55, no. 5, pp. 72–79, May 2017.

[6] O. U. Akgül, I. Malanchini, and A. Capone, "Dynamic resource trading in sliced mobile networks," *IEEE Trans. Netw. Service Manag.*, vol. 16, no. 1, pp. 220–233, Mar. 2019.

[7] R. Tang, J. Zhao, H. Qu, and Z. Zhang, "User-centric QoS provisioning for heterogeneous D2D multimedia flows with dense spectral reuse," in *Proc. IEEE Globecom Workshops (GC Wkshps)*, Dec. 2016, pp. 1–7.

[8] *Study on New Radio (NR) Access Technology (Release 14)*, document 3GPP TR 38.912 version 14.0.0, Jun. 2017. Accessed: Sep. 11, 2017. [Online]. Available: https://portal.3gpp.org/desktopmodules/Specifications/SpecificationDetails.aspx?specificationId=3059

[9] D. Li and X. Sun, *Nonlinear Integer Programming* (Mathematics International Series in Operations Research & Management Science). New York, NY, USA: Springer, 2006.

[10] C. Buchheim and G. Rinaldi, "Efficient reduction of polynomial zero-one optimization to the quadratic case," *SIAM J. Optim.*, vol. 18, no. 4, pp. 1398–1413, 2008.

[11] E. Rodríguez-Heck, "Linear and quadratic reformulations of nonlinear optimization problems in binary variables," Ph.D. dissertation, QuantOM, HEC Manage. School, Univ. Liège, Liège, Belgium, 2018.

[12] F. Wang and D. P. Landau, "Efficient, multiple-range random walk algorithm to calculate the density of states," *Phys. Rev. Lett.*, vol. 86, pp. 2050–2053, Mar. 2001.

[13] S. Ermon, C. P. Gomes, and B. Selman, "Computing the density of states of Boolean formulas," in *Principles and Practice of Constraint Programming—CP 2010*, D. Cohen, Ed. Berlin, Germany: Springer, 2010, pp. 38–52.

[14] D. Achlioptas, A. Naor, and Y. Peres, "Rigorous location of phase transitions in hard optimization problems," *Nature*, vol. 435, no. 7043, pp. 759–764, 2005.

[15] W. Wang, Y. Chen, and J. Huang, "Heterogeneous preferences, decision-making capacity, and phase transitions in a complex adaptive system," *Proc. Nat. Acad. Sci. USA*, vol. 106, no. 21, pp. 8423–8428, 2009.

[16] *Study on Management and Orchestration of Network Slicing for Next Generation Network*, document 3GPP TR 28.801 Release 15, Jan. 2018.

[17] O. Sallent, J. Pérez-Romero, R. Ferrús, and R. Agustí, "On radio access network slicing from a radio resource management perspective," *IEEE Wireless Commun.*, vol. 24, no. 5, pp. 166–174, Oct. 2017.

[18] R. Ferrus, O. Sallent, J. P. Romero, and R. Agusti, "On 5G radio access network slicing: Radio interface protocol features and configuration," *IEEE Commun. Mag.*, vol. 56, no. 5, pp. 184–192, May 2018.

[19] C. Campolo, A. Molinaro, A. Iera, and F. Menichella, "5G network slicing for vehicle-to-everything services," *IEEE Wireless Commun.*, vol. 24, no. 6, pp. 38–45, Dec. 2017.

[20] C. Liang and F. R. Yu, "Distributed resource allocation in virtualized wireless cellular networks based on ADMM," in *Proc. IEEE Conf. Comput. Commun. Workshops (INFOCOM WKSHPS)*, Apr. 2015, pp. 360–365.

[21] P. L. Vo, M. N. H. Nguyen, T. A. Le, and N. H. Tran, "Slicing the edge: Resource allocation for RAN network slicing," *IEEE Wireless Commun. Lett.*, vol. 7, no. 6, pp. 970–973, Dec. 2018.

[22] N. Van Huynh, D. T. Hoang, D. N. Nguyen, and E. Dutkiewicz, "Optimal and fast real-time resource slicing with deep dueling neural networks," *IEEE J. Sel. Areas Commun.*, vol. 37, no. 6, pp. 1455–1470, Jun. 2019.

[23] T. Guo and A. Suárez, "Enabling 5G RAN slicing with EDF slice scheduling," *IEEE Trans. Veh. Technol.*, vol. 68, no. 3, pp. 2865–2877, Mar. 2019.

[24] R. Shrivastava, K. Samdanis, and V. Sciancalepore, "Towards service-oriented soft spectrum slicing for 5G TDD networks," *J. Netw. Comput. Appl.*, vol. 137, pp. 78–90, Jul. 2019.

[25] V. Sciancalepore, M. Di Renzo, and X. Costa-Perez, "STORNS: Stochastic radio access network slicing," 2019, *arXiv:1901.05336*. [Online]. Available: https://arxiv.org/abs/1901.05336

[26] D. Bega, M. Gramaglia, M. Fiore, A. Banchs, and X. Costa-Perez, "DeepCog: Cognitive network management in sliced 5G networks with deep learning," in *Proc. 38th IEEE Int. Conf. Comput. Commun. (INFOCOM)*, Apr./May 2019, pp. 280–288.

[27] V. Sciancalepore, L. Zanzi, X. Costa-Perez, and A. Capone, "ONETS: Online network slice broker from theory to practice," 2018, *arXiv:1801.03484*. [Online]. Available: https://arxiv.org/abs/1801.03484

[28] H. Jin, H. Lu, Y. Jin, and C. Zhao, "IVCN: Information-centric network slicing optimization based on NFV in fog-enabled RAN," *IEEE Access*, vol. 7, pp. 69667–69686, 2019.

[29] M. Jiang, M. Kondoluci, and T. Mahmoodi, "Network slicing management & prioritization in 5G mobile systems," in *Proc. Eur. Wireless Conf.*, May 2016, pp. 1–6.

[30] G. Zhang, K. Yang, H. Jiang, X. Lu, K. Xu, and L. Zhang, "Equilibrium price and dynamic virtual resource allocation for wireless network virtualization," *Mobile Netw. Appl.*, vol. 22, no. 3, pp. 564–576, Jun. 2017.

[31] S. Parsaeefard, R. Dawadi, M. Derakhshani, and T. Le-Ngoc, "Joint user-association and resource-allocation in virtualized wireless networks," *IEEE Access*, vol. 4, pp. 2738–2750, 2016.

[32] B. Niu, Y. Zhou, H. Shah-Mansouri, and V. W. Wong, "A dynamic resource sharing mechanism for cloud radio access networks," *IEEE Trans. Wireless Commun.*, vol. 15, no. 12, pp. 8325–8338, Dec. 2016.

[33] J. Ye and Y.-J. Zhang, "Pricing-based resource allocation in virtualized cloud radio access networks," *IEEE Trans. Veh. Technol.*, vol. 68, no. 7, pp. 7096–7107, Jul. 2019.

[34] Y. Xiao, M. Hirzallah, and M. Krunz, "Distributed resource allocation for network slicing over licensed and unlicensed bands," *IEEE J. Sel. Areas Commun.*, vol. 36, no. 10, pp. 2260–2274, Oct. 2018.

[35] K. Wang, F. R. Yu, and H. Li, "Information-centric virtualized cellular networks with device-to-device communications," *IEEE Trans. Veh. Technol.*, vol. 65, no. 11, pp. 9319–9329, Nov. 2016.

[36] Q. Ye, W. Zhuang, S. Zhang, A-L. Jin, X. Shen, and X. Li, "Dynamic radio resource slicing for a two-tier heterogeneous wireless network," *IEEE Trans. Veh. Technol.*, vol. 67, no. 10, pp. 9896–9910, Oct. 2018.

[37] T. LeAnh, N. H. Tran, D. T. Ngo, and C. S. Hong, "Resource allocation for virtualized wireless networks with backhaul constraints," *IEEE Commun. Lett.*, vol. 21, no. 1, pp. 148–151, Jan. 2017.

[38] M. Srinivasan and S. R. Murthy, "Efficient spectrum slicing in 5G networks: An overlapping coalition formation approach," *IEEE Trans. Mobile Comput.*, to be published.

[39] M. Yan, G. Feng, J. Zhou, Y. Sun, and Y. Liang, "Intelligent resource scheduling for 5G radio access network slicing," *IEEE Trans. Veh. Technol.*, vol. 68, no. 8, pp. 7691–7703, Aug. 2019.

[40] K. Zhu and E. Hossain, "Virtualization of 5G cellular networks as a hierarchical combinatorial auction," *IEEE Trans. Mobile Comput.*, vol. 15, no. 10, pp. 2640–2654, Oct. 2016.

[41] K. Zhu, Z. Cheng, B. Chen, and R. Wang, "Wireless virtualization as a hierarchical combinatorial auction: An illustrative example," in *Proc. IEEE Wireless Commun. Netw. Conf. (WCNC)*, Mar. 2017, pp. 1–6.

[42] S. Parsaeefard, R. Dawadi, M. Derakhshani, T. Le-Ngoc, and M. Baghani, "Dynamic resource allocation for virtualized wireless networks in massive-MIMO-aided and fronthaul-limited C-RAN," *IEEE Trans. Veh. Technol.*, vol. 66, no. 10, pp. 9512–9520, Oct. 2017.

[43] J. García-Rois, B. Lorenzo, F. J. González-Castaño, F. Gil-Castiñeira, and J. Wu, "Slice allocation and pricing framework for virtualized millimeter wave cellular networks," *IEEE Access*, vol. 7, pp. 86349–86366, 2019.

[44] M. S. Parwez and D. B. Rawat, "Resource allocation in adaptive virtualized wireless networks with mobile edge computing," in *Proc. IEEE Int. Conf. Commun. (ICC)*, May 2018, pp. 1–7.

[45] L. Gao, P. Li, Z. Pan, N. Liu, and X. You, "Virtualization framework and VCG based resource block allocation scheme for lte virtualization," in *Proc. IEEE 83rd Veh. Technol. Conf. (VTC Spring)*, May 2016, pp. 1–6.

[46] C.-Y. Chang, N. Nikaein, and T. Spyropoulos, "Radio access network resource slicing for flexible service execution," in *Proc. IEEE Conf. Comput. Commun. Workshops (INFOCOM)*, Apr. 2018, pp. 668–673.

[47] M. I. Kamel, L. B. Le, and A. Girard, "LTE wireless network virtualization: Dynamic slicing via flexible scheduling," in *Proc. IEEE Veh. Tech. Conf. (VTC)*, Sep. 2014, pp. 1–5.

[48] L. Tang, Q. Tan, Y. Shi, C. Wang, and Q. Chen, "Adaptive virtual resource allocation in 5G network slicing using constrained Markov decision process," *IEEE Access*, vol. 6, pp. 61184–61195, 2018.

[49] A. T. Z. Kasgari and W. Saad, "Stochastic optimization and control framework for 5G network slicing with effective isolation," in *Proc. 52nd Annu. Conf. Inf. Sci. Syst. (CISS)*, Mar. 2018, pp. 1–6.

[50] Y. L. Lee, J. Loo, T. C. Chuah, and L.-C. Wang, "Dynamic network slicing for multitenant heterogeneous cloud radio access networks," *IEEE Trans. Wireless Commun.*, vol. 17, no. 4, pp. 2146–2161, Apr. 2018.

[51] A. Papa, M. Klügel, L. Goratti, T. Rasheed, and W. Kellerer, "Optimizing dynamic RAN slicing in programmable 5G networks," in *Proc. IEEE Int. Conf. Commun. (ICC)*, May 2019, pp. 1–7.

[52] J. Gang and V. Friderikos, "Inter-tenant resource sharing and power allocation in 5G virtual networks," *IEEE Trans. Veh. Technol.*, vol. 68, no. 8, pp. 7931–7943, Aug. 2019.

[53] D. Wu, Z. Zhang, S. Wu, J. Yang, and R. Wang, "Biologically inspired resource allocation for network slices in 5G-enabled Internet of Things," *IEEE Internet Things J.*, to be published.

[54] P. Popovski, K. F. Trillingsgaard, O. Simeone, and G. Durisi, "5G wireless network slicing for eMBB, URLLC, and mMTC: A communication-theoretic view," *IEEE Access*, vol. 6, pp. 55765–55779, 2018.
[55] L. Tang, X. Zhang, H. Xiang, Y. Sun, and M. Peng, "Joint resource allocation and caching placement for network slicing in fog radio access networks," in *Proc. IEEE 18th Int. Workshop Signal Process. Adv. Wireless Commun. (SPAWC)*, Jul. 2017, pp. 1–6.
[56] G. Sun, Z. T. Gebrekidan, G. O. Boateng, D. Ayepah-Mensah, and W. Jiang, "Dynamic reservation and deep reinforcement learning based autonomous resource slicing for virtualized radio access networks," *IEEE Access*, vol. 7, pp. 45758–45772, 2019.
[57] G. Sun, K. Xiong, G. O. Boateng, D. Ayepah-Mensah, G. Liu, and W. Jiang, "Autonomous resource provisioning and resource customization for mixed traffics in virtualized radio access network," *IEEE Syst. J.*, vol. 13, no. 3, pp. 2454–2465, Sep. 2019.
[58] B. Han, J. Lianghai, and H. D. Schotten, "Slice as an evolutionary service: Genetic optimization for inter-slice resource management in 5G networks," *IEEE Access*, vol. 6, pp. 33137–33147, 2018.
[59] D. Bega, M. Gramaglia, A. Banchs, V. Sciancalepore, K. Samdanis, and X. Costa-Perez, "Optimising 5G infrastructure markets: The business of network slicing," in *Proc. IEEE Conf. Comput. Commun. (INFOCOM)*, May 2017, pp. 1–9.
[60] Z. Chang, D. Zhang, T. Hamalainen, Z. Han, and T. Ristaniemi, "Incentive mechanism for resource allocation in wireless virtualized networks with multiple infrastructure providers," *IEEE Trans. Mobile Comput.*, to be published.
[61] O. U. Akgul, I. Malanchini, and A. Capone, "Anticipatory resource allocation and trading in a sliced network," in *Proc. IEEE Int. Conf. Commun. (ICC)*, May 2019, pp. 1–7.
[62] H. Schawe, R. Bleim, and A. K. Hartmann, "Phase transitions of the typical algorithmic complexity of the random satisfiability problem studied with linear programming," *PLoS ONE*, vol. 14, no. 4, Apr. 2019, Art. no. e0215309.
[63] R. V. Rasmussen and M. A. Trick, "A Benders approach for the constrained minimum break problem," *Eur. J. Oper. Res.*, vol. 177, no. 1, pp. 198–213, Feb. 2007.
[64] S. Bian, J. Song, M. Sheng, Z. Shao, J. He, Y. Zhang, Y. Li, and I. Chih-Lin, "Sum-rate maximization in OFDMA downlink systems: A joint subchannels, power, and MCS allocation approach," in *Proc. IEEE 25th Annu. Int. Symp. Pers., Indoor, Mobile Radio Commun. (PIMRC)*, Sep. 2014, pp. 1073–1077.
[65] Y. Wang, B. Liang, and Y. Xu, "A two-stage rank selection scheme in downlink CoMP transmission networks," in *Proc. IEEE Int. Conf. Commun. (ICC)*, May 2016, pp. 1–6.
[66] *NR and NG-RAN Overall Description; Stage 2 (Release 15)*, document 3GPP TS 38.300, Jun. 2018. Accessed: Sep. 13, 2018. [Online]. Available: https://portal.3gpp.org/desktopmodules/Specifications/SpecificationDetails.aspx?specificationId=3191
[67] A. Karimi, K. I. Pedersen, N. H. Mahmood, J. Steiner, and P. Mogensen, "5G centralized multi-cell scheduling for URLLC: Algorithms and system-level performance," *IEEE Access*, vol. 6, pp. 72253–72262, 2018.
[68] A. A. Zaidi, R. Baldemair, H. Tullberg, H. Bjorkegren, L. Sundstrom, J. Medbo, C. Kilinc, and I. Da Silva, "Waveform and numerology to support 5G services and requirements," *IEEE Commun. Mag.*, vol. 54, no. 11, pp. 90–98, Nov. 2016.
[69] K. Cho and D. Yoon, "On the general BER expression of one- and two-dimensional amplitude modulations," *IEEE Trans. Commun.*, vol. 50, no. 7, pp. 1074–1080, Jul. 2002.
[70] *NR; Physical Layer Procedures for Data*, document 3GPP TS 38.214 version 15.2.0 Release 15, Sep. 2018.
[71] M. Jünger, T. M. Liebling, D. Naddef, G. L. Nemhauser, W. R. Pulleyblank, G. Reinelt, G. Rinaldi, and L. A. Wolsey, "Nonlinear integer programming," in *50 Years of Integer Programming 1958–2008: From the Early Years to the State-of-the-Art*, M. Jünger, Ed. Berlin, Germany: Springer, 2010.
[72] H. Q. Ngo, A. Ashikhmin, H. Yang, E. G. Larsson, and T. L. Marzetta, "Cell-free massive MIMO versus small cells," *IEEE Trans. Wireless Commun.*, vol. 16, no. 3, pp. 1834–1850, Mar. 2017.
[73] N. Metropolis, A. W. Rosenbluth, M. N. Rosenbluth, A. H. Teller, and E. Teller, "Equation of state calculations by fast computing machines," *J. Chem. Phys.* vol. 21, no. 6, pp. 1087–1092, 1953.
[74] P. Ojeda-May and M. E. Garcia, "Electric field-driven disruption of a native β-sheet protein conformation and generation of a helix-structure," *Biophys. J.*, vol. 99, no. 2, pp. 595–599, 2010.
[75] N. McBride, J. Bulava, C. Galiotto, N. Marchetti, I. Macaluso, and L. Doyle, "Degeneracy estimation in interference models on wireless networks," *Phys. A, Stat. Mech. Appl.*, vol. 469, pp. 540–550, Mar. 2017.
[76] M. S. Shell, P. G. Debenedetti, and A. Z. Panagiotopoulos, "Generalization of the Wang–Landau method for off-lattice simulations," *Phys. Rev. E, Stat. Phys. Plasmas Fluids Relat. Interdiscip. Top.*, vol. 66, no. 5, Nov. 2002, Art. no. 056703.
[77] A. Tröster and C. Dellago, "Wang–Landau sampling with self-adaptive range," *Phys. Rev. E, Stat. Phys. Plasmas Fluids Relat. Interdiscip. Top.*, vol. 71, Jun. 2005, Art. no. 066705.
[78] A. C. K. Farris, G. Shi, T. Wüst, and D. P. Landau, "The role of chain-stiffness in lattice protein models: A replica-exchange Wang–Landau study," *J. Chem. Phys.*, vol. 149, no. 12, 2018, Art. no. 125101.
[79] L. Y. Barash, M. A. Fadeeva, and L. N. Shchur, "Control of accuracy in the Wang–Landau algorithm," *Phys. Rev. E, Stat. Phys. Plasmas Fluids Relat. Interdiscip. Top.*, vol. 96, Oct. 2017, Art. no. 043307.
[80] R. E. Belardinelli and V. D. Pereyra, "Wang–Landau algorithm: A theoretical analysis of the saturation of the error," *J. Chem. Phys.*, vol. 127, no. 18, 2007, Art. no. 184105.
[81] F. Liang, C. Liu, and R. J. Carroll, "Stochastic approximation in Monte Carlo computation," *J. Amer. Stat. Assoc.*, vol. 102, no. 477, pp. 305–320, 2007.
[82] L. N. Shchur, "On properties of the Wang–Landau algorithm," *J. Phys., Conf. Ser.*, vol. 1252, Jun. 2019, Art. no. 012010.
[83] V. S. Abhayawardhana, I. J. Wassell, D. Crosby, M. P. Sellars, and M. G. Brown, "Comparison of empirical propagation path loss models for fixed wireless access systems," in *Proc. IEEE 61st Veh. Technol. Conf.*, vol. 1, May 2005, pp. 73–77.

J. J. ESCUDERO-GARZÁS received the Ph.D. degree in electrical engineering from the Universidad Carlos III de Madrid (UC3M). From 1997 to 2002, he was a Provisioning Engineer with Spanish telcos and the Head of the Communications Network Maintenance Department. He has been a Faculty Member with the Department of Signal Theory and Communications, UC3M. He was also a Postdoctoral Fellow with the Universitat Autònoma de Barcelona, from 2010 to 2012, and a Visiting Researcher with the University of Virginia, in 2013, and the University of Florida, in 2017. His research interests include optimization of wireless communication systems and resource management for 5G networks.

CARLOS BOUSOÑO-CALZÓN received the degree in engineering and the Ph.D. degree in telecommunication from the Universidad Carlos III de Madrid (UC3M), Spain. He was with Telefónica I+D, Madrid, Spain, and BT Research, Ipswich, U.K., while doing his Ph.D. degree. He was an Assistant Professor with the University of Sevilla and then joined UC3M, where he is currently an Associate Professor with the Department of Signal Theory and Communications. From 2007 to 2009, he served as a Seconded National Expert for the FET-Proactive Unit, European Commission. His research interests include information processing for complex systems and their social applications.

ALFREDO GARCÍA received the degrees in electrical engineering from the Universidad de los Andes, Colombia, in 1991, and the Université Paul Sabatier, Toulouse, France, in 1992, and the Ph.D. degree in industrial and operations engineering from the University of Michigan, in 1997. From 1998 to 2000, he served as Commissioner with the Colombian Energy Regulatory Commission. From 2001 to 2017, he was a member of the faculty with the University of Virginia and the University of Florida. His research interests include game theory, and dynamic optimization with applications in electricity and communication networks.